ADVANCED MATERIALS INTERFACES
Open Access
www.advmatinterfaces.de

Polyoxometalate Aerogels Formed by Organofunctionalized Anderson Polyoxometalates as Low Molecular Weight Gelators

Garima Sachdeva, Salam Maloul, Julia Zolg, Riccarda Müller, Mihail Mondeshki, Elnaz Ebrahimi, Dhouha Abid, Soressa Abera Chala, Christof Neumann, Andrey Turchanin, Johannes Biskupek, Ute Kaiser, Kerstin Leopold, and Carsten Streb**

Polyoxometalate-based aerogels, built through supramolecular interactions and metal coordination, have the potential to expand the field of smart materials. Here, the first example of the conversion of an Anderson-polyoxometalate-based organogel into a catalytically active aerogel is reported. The polyoxometalate organogel is formed by the reaction of $ZnCl_2$ with the TRIS-functionalized Anderson polyoxometalate $(nBu_4N)_3[MnMo_6O_{18}\{(OCH_2)_3CNH_2\}_2]$. Conversion of the organogel into the aerogel is achieved by a scalable freeze-drying procedure. A range of experimental methods are employed to follow the conversion of the POM into the organogel and aerogel, and insights into the role of the polyoxometalate, the metal salt, and the solvent are reported. The catalytic activity of the aerogel for selective alcohol oxidations (model compounds: benzyl alcohol, furfuryl alcohol, octanol) is reported together with initial recyclability studies. A conversion yield of 30% for benzaldehyde is achieved using aerogel as a catalyst. The study opens the door to (multi-)functional polyoxometalate-based aerogels for sorption, separation, catalysis, and energy technologies.

1. Introduction

Supramolecular gels are a promising class of functional soft materials with unique structure and function.[1–3] Metallogels in particular are attractive, as classical coordination chemistry between metal cations and suitable organic ligands can be used to design and tune the gel properties and reactivities.[4–6] Further, this linkage is assisted via non-covalent interactions such as hydrogen bonding, electrostatic, or hydrophobic interactions.[7,8] This has led to applications ranging from catalysis and sensing to optoelectronics and magnetism.[9–13] Rational design of metallogelators, therefore, is challenging, and significant attempts in molecular synthesis and design are requisite to create systems in which metal is accountable for both cross-linking and coordination.[14,15] Metallogels can also be converted into technologically important aerogels[16,17] using freeze-drying.[18] This approach removes the solvent from the gel structure while maintaining its 3D architecture. Aerogels are unique materials that feature high specific surface area, low density, and hierarchical pore structures.[19] The exceptional features of the aerogels have led to their development in the areas of catalysis,[20] biomedicine,[21] energy storage,[22] and

G. Sachdeva, M. Mondeshki, E. Ebrahimi, D. Abid, S. A. Chala, C. Streb
Department of Chemistry
Johannes Gutenberg University Mainz
Duesbergweg 10–14, 55128 Mainz, Germany
E-mail: carsten.streb@uni-mainz.de

S. Maloul, J. Zolg, C. Streb
Institute of Inorganic Chemistry I
Ulm University
Albert-Einstein-Allee 11 D, 89081 Ulm, Germany

The ORCID identification number(s) for the author(s) of this article can be found under https://doi.org/10.1002/admi.202500597

DOI: 10.1002/admi.202500597

R. Müller, K. Leopold
Institute of Analytical and Bioanalytical Chemistry
Ulm University
Albert-Einstein-Allee 11, 89081 Ulm, Germany
E-mail: kerstin.leopold@uni-ulm.de

C. Neumann, A. Turchanin
Friedrich Schiller University Jena
Institute of Physical Chemistry
Lessigstraße 10, 07743 Jena, Germany

A. Turchanin
Center for Energy and Environmental Chemistry Jena (CEEC Jena)
Philosophenweg 7a, 07743 Jena, Germany

J. Biskupek, U. Kaiser
Electron Microscopy Group of Materials Science
Ulm University
Albert-Einstein-Allee 11, 89081 Ulm, Germany

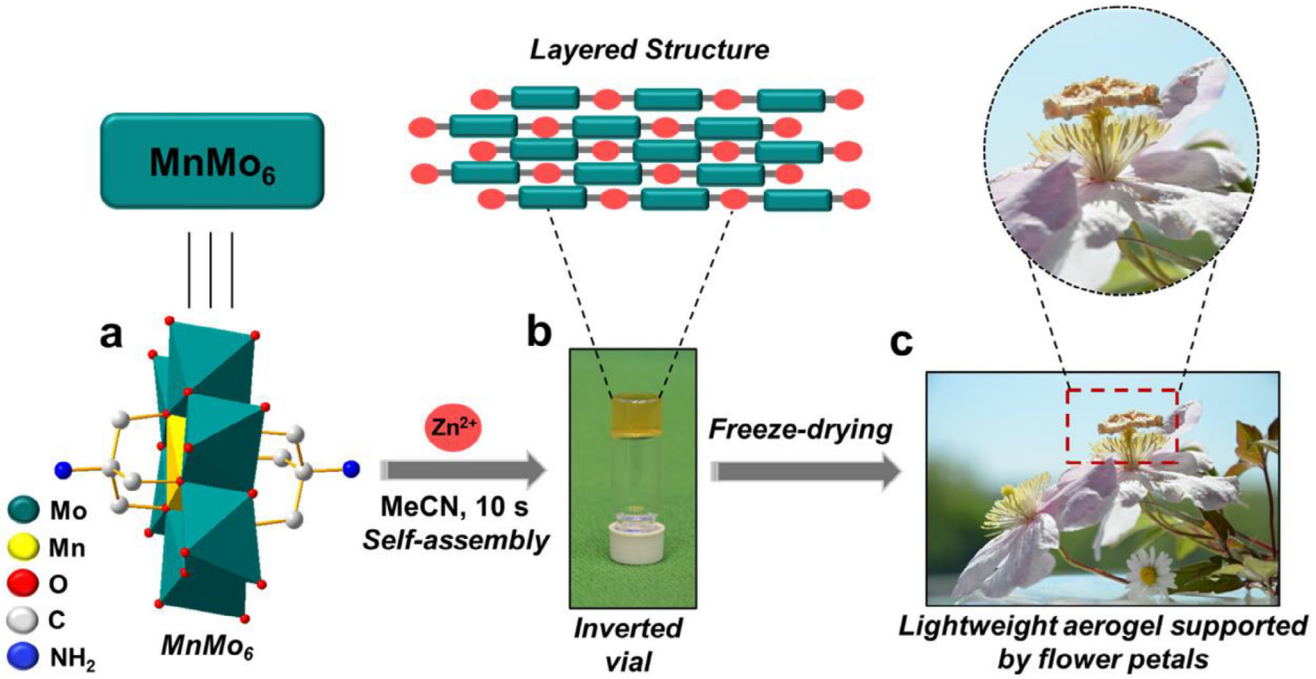

Figure 1. a) Illustration of the TRIS-functionalized Anderson POM low molecular weight gelator. b) Illustration of the organogel formation. c) Photograph of the low-weight aerogel placed on top of a flower.

water treatment.[23] Furthermore, the use of numerous materials and their modification in the construction of aerogels has broadened their application area, ranging from photocatalysis to the food industry.[24] Recently, metal-based aerogels have been widely explored for their unique function in catalysis,[25] engineering materials,[26] and sensing.[27]

In particular, molecular metal oxide anions, so-called polyoxometalates (POMs),[28] have recently been put forward as a new low molecular weight gelator class for the design of metallogels. POMs are versatile molecules having tunable structures and reactivities. In addition, they are excellent electron reservoirs and possess rich redox chemistry, making them ideal for catalysis, energy storage, and conversion.[29,30] POMs can be cross-linked by a number of interactions, including electrostatics or hydrogen bonding. Moreover, POMs can be covalently functionalized with a range of organic ligands, which opens the pathway to use the ligands for further linkage and to control the properties of the resulting gels.[31] Inspired by these possibilities, Zhou, Wang, and colleagues have reported metallogels based on Keggin-type anions $[PMo_{12}O_{40}]^{3-}$ which were employed as anode materials for lithium-ion batteries and displayed promising rate capability, high reversible capacity, and decent cycling stability.[32] Izzet, Bo, and co-workers have developed dumbbell-type dimers linked via Co(II) or Co(III) made of Keggin and Dawson POMs functionalized with terpyridine ligands. The resulting metallogels showed intriguing solvent exchange properties, opening the path to form hydrogels.[33]

One prototype gel-forming POM is the organofunctionalized Anderson-Evans polyoxometalate[34] $[XMo_6O_{18}\{RC(CH_2O)_3\}_2]^{3-}$ (where X = Mn, Fe, Co, and R = $-NH_2$, $-CH_3$, $-CH_2OH$) which features two organic ligands arranged in a linear fashion on opposite sides of the cluster, tethered by tris-alkoxide groups (**Figure 1a**). Pioneering work on Anderson-based gels was performed by Hasenknopf and colleagues, who reported the formation of an anisotropic supramolecular gel showing good thermal stability and birefringence.[35] The gel was formed by the coordination of Pd(II) salt to Anderson anions covalently functionalized with pyridyl moieties.[35] In a related study, Li and co-workers showed that the intermolecular combination of pyridyl functionalized Anderson POM with suitable dicarboxylic acids resulted in the immediate formation of a supramolecular gel, which showed rapid stimuli-responsiveness to organic acids and bases.[36] More recently, Izzet, Merland, Davidson, Solé-Daura, and co-workers designed supramolecular metallogels by linking terpyridine-functionalized Anderson anions with Zn(II) or Co(II) cations. The hybrid gels exhibited intriguing properties, including luminescence, birefringence, and spin-crossover.[37] To date, to the best of our knowledge, the conversion of purely POM-based metallogels into aerogels has not been reported. However, there is widespread interest in POM-containing aerogels, as they have been utilized in areas ranging from electrocatalysis[38] and batteries[39] to pollutant removal[40] and aerospace materials.[41] The structural and chemical tunability and redox behavior offered by POM make them an ideal candidate for utilization in several applications as compared to conventional aerogels.[42,43]

Furthermore, in recent years, Anderson-Evans POMs have been widely studied as catalysts for several oxidation reactions, showing their potential to oxidize several organic compounds, such as thioanisoles and furan-based chemicals.[44,45] Building on these studies, we now report the use of POM-based aerogel in the oxidation of primary alcohols, paving the path to using POM-based porous catalysts in the transformation of organic reactions.

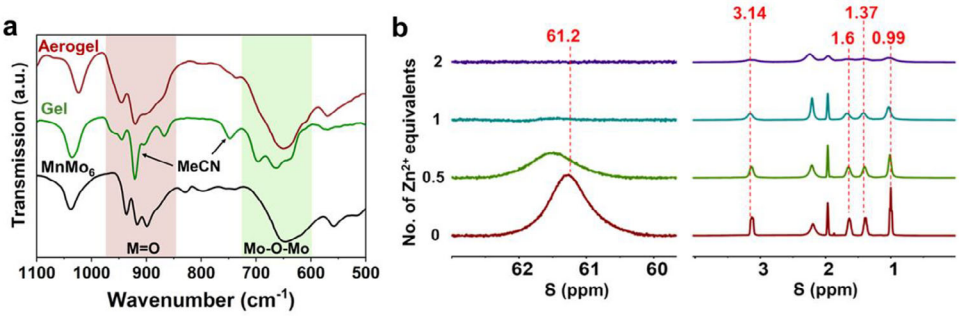

Figure 2. a) Stacked FT-IR spectra of the organogel and the aerogel (1), and their comparison with the distinctive peaks of reference $MnMo_6$. b) Stacked ^1H NMR spectra of deuterated acetonitrile solutions of $MnMo_6$ and varying equivalents of Zn(II). Conditions: $[MnMo_6]$ = 63.7 mM, and $[ZnCl_2]$ = 82.8 mM, solvent = acetonitrile-d_3.

Herein, we report the development of a POM-based organogel, formed within 10 s by reaction of $ZnCl_2$ with TRIS-functionalized Anderson POM in acetonitrile solution. The resulting organogel can easily be converted into an aerogel by freeze-drying. We provide a full characterization of the aerogel and demonstrate its principal suitability for selective alcohol oxidation reactions using benzyl alcohol, furfuryl alcohol, and octanol as model substrates. In addition, initial insights into the scope of gel formation are presented with a focus on the role of the POM, the $ZnCl_2$, and the solvent.

2. Results and Discussion

2.1. Catalyst Synthesis and Characterization

Briefly, the POM-based organogel was prepared by combining acetonitrile solutions of $ZnCl_2$ and the TRIS-functionalized Anderson anion $(n\mathrm{Bu_4N})_3[MnMo_6O_{18}\{(OCH_2)_3CNH_2\}_2]$[46] (hereafter: $MnMo_6$). Reaction of both solutions resulted in near-instantaneous gel formation (gelation time *ca.* 10 s). The vial inversion test[47,48] was used to demonstrate the stability and viscoelasticity of the gel, see Figure 1b. Next, the organogel was converted into an aerogel (1) by freeze-drying (for synthetic and characterization details of the organogel and 1, see Supporting Information).

The structural changes occurring during gelation and freeze-drying were investigated using FT-IR spectroscopy (**Figure 2a**). Upon gelation, both the bridging Mo—O—Mo band (*ca.* 650 cm^{-1}) as well as the terminal Mo═O feature (890–950 cm^{-1}) showed minor, but characteristic changes (peak splitting, peak broadening). These changes indicate that the outer oxo ligands of $MnMo_6$ are involved in the gelation process. In addition, the presence of the bands at *ca.* 749 and 920 cm^{-1} corresponding to the acetonitrile molecules[49,50] suggests the possibility of solvent-coordination for the stabilization of the Zn(II) center. Further, upon freeze-drying and removal of the MeCN solvent, further broadening of these signals is observed, in particular for the band located at *ca.* 900 cm^{-1}. This indicates that further molecular-level structure changes of the gel network occur upon freeze-drying. One plausible interpretation of these findings is that acetonitrile-stabilized Zn(II) coordinates to the oxo ligands of $MnMo_6$ to trigger the gelation process. Upon solvent removal, minor structural changes at the Zn(II) center might occur, which would be in line with the observed spectroscopic changes reported.

To gain more structural insights into the gelation process, we performed ^1H NMR spectroscopic titrations, where 0 to 2 molar equivalents of $ZnCl_2$ were added to the $MnMo_6$ solution in deuterated acetonitrile (Figure 2b). Note that the methylene protons of the TRIS-NH_2 experience a significant paramagnetic shift due to the effect of the Mn(III) center of the Anderson POM.[46] Upon the addition of increasing amounts of $ZnCl_2$, we observe a broadening and intensity decrease of all ^1H NMR signals. The reduced molecular mobility as a result of gelation results in the partial reintroduction of the anisotropic chemical shift and dipole–dipole couplings, which affect the spectral lines. Previous reports also have shown similar observations of line broadening of characteristic peaks, where Keggin-type POMs have triggered the hydrogel formation with γ-cyclodextrin.[51]

The thermal stability of 1 was examined by thermogravimetric analysis (TGA) in an air atmosphere (Figure S1, Supporting Information). A significant weight loss of 27.6% (calculated: 28.3%) is observed between 200 and 385 °C, which is attributed to the loss of three $n\mathrm{Bu_4N^+}$ cations. A second weight loss of 18.4% between 410 to 555 °C is associated with the simultaneous decomposition of the TRIS moieties[52] and volatilization of $ZnCl_2$.[53,54] This data was supported by CHN elemental analysis, which is in line with the presence of three $n\mathrm{Bu_4N^+}$ cations and two TRIS moieties per formula unit (Table S6, Supporting Information). Next, the elemental composition and oxidation states at the surface of 1 were investigated by X-ray photoelectron spectroscopy (XPS). The survey XP spectrum verifies the presence of all expected elements (Figure S2, Supporting Information). The deconvoluted high-resolution Mo 3d spectrum (**Figure 3a**) shows two peaks at binding energies of 232.4 and 235.6 eV corresponding to Mo $3d_{5/2}$ and Mo $3d_{3/2}$, respectively, indicating the presence of Mo(VI).[55] A spin-orbit coupled doublet of Mn 2p at binding energies of 640.9 and 652.7 eV is assigned to Mn $2p_{3/2}$ and Mn $2p_{1/2}$ of Mn(III), respectively (Figure 3b).[56,57] The Cl 2p spectrum (Figure 3c) shows binding energies at 200.2 eV (Cl $2p_{1/2}$) and 198.5 eV (Cl $2p_{3/2}$), assigned to Cl-Zn coordination.[58] Moreover, the Zn 2p XP spectrum revealed two peaks at 1045.3 and 1022.4 eV, which are assigned to Zn $2p_{1/2}$ and Zn $2p_{3/2}$ signals of the Zn(II) species (Figure 3d).[59,60]

The morphology of 1 was studied by scanning electron microscopy (SEM, **Figure 4a,b**). This analysis showed a

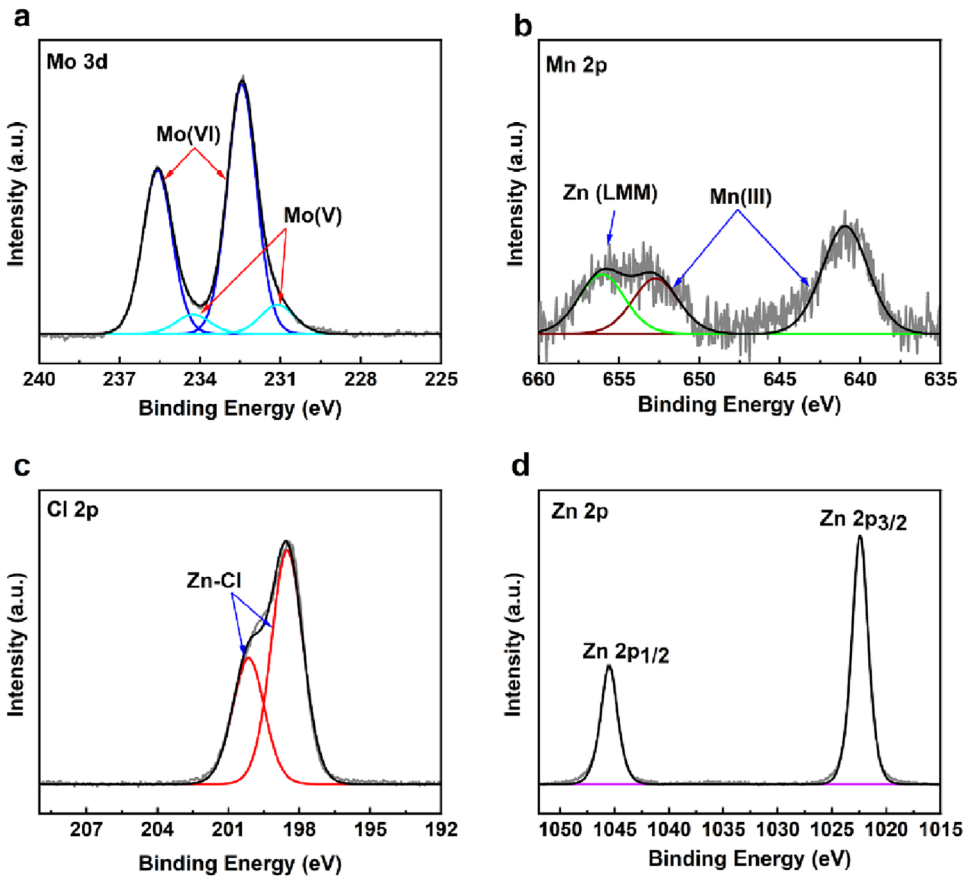

Figure 3. Deconvoluted high-resolution a) Mo 3d, b) Mn 2p, c) Cl 2p, d) Zn 2p XP spectra for 1.

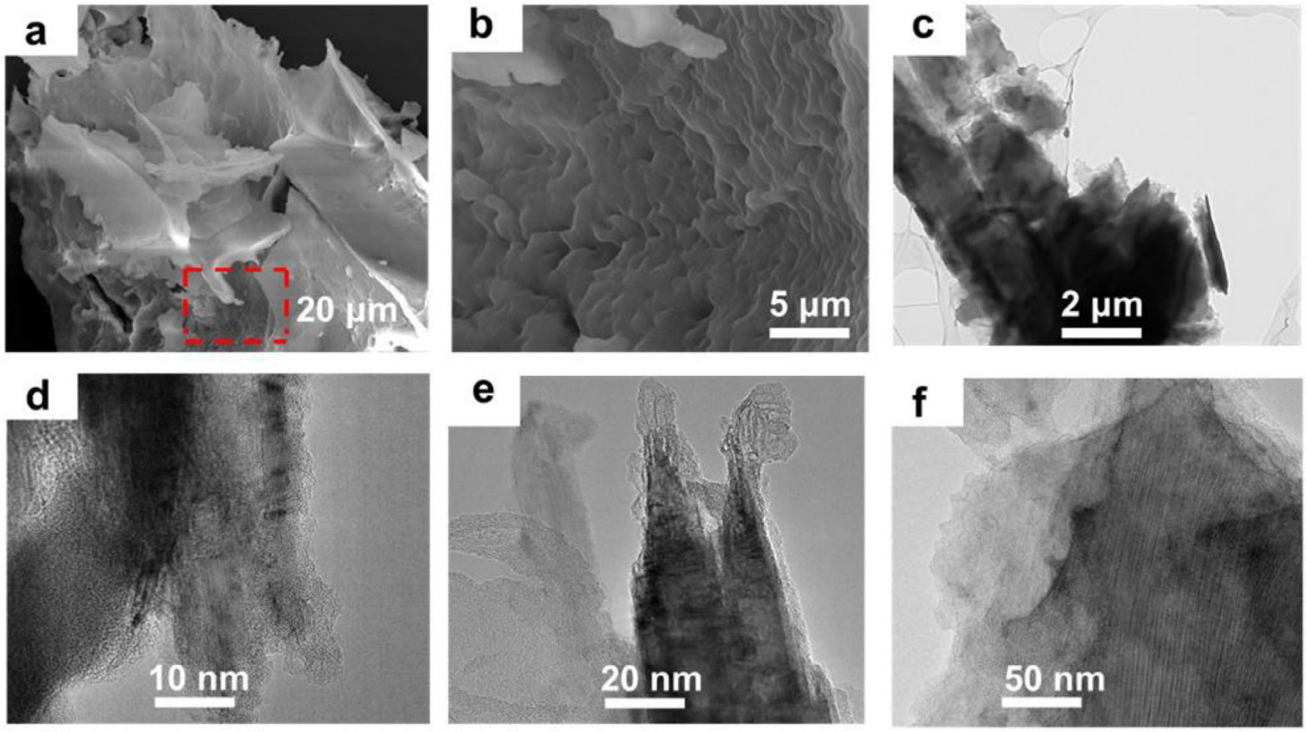

Figure 4. Electron microscopy of 1. a) SEM image, b) magnification of the selected area (in a red rectangle), c,d) TEM images, e,f) HRTEM images.

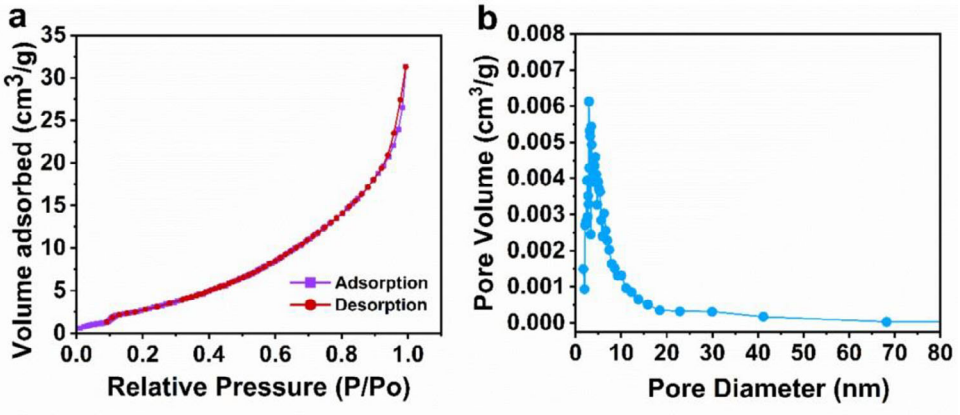

Figure 5. Representative Histograms of a) N_2 adsorption-desorption isotherm, b) Pore size distribution of 1.

layered structure composed of stacked and agglomerated sheets. To obtain further insights into the morphological and structural properties of as synthesized 1, transmission electron microscopy (TEM), high-resolution transmission electron microscopy (HRTEM), and scanning-transmission electron microscopy (STEM) together with energy dispersive X-ray spectroscopy (EDS) were employed. As shown in Figure 4c,d, the structure of 1 consists of thin and long fibrous sheets that appear stacked. Furthermore, HRTEM analysis (Figure 4e,f) indicates the existence of both long fibrous and layered structures, which might be due to the supramolecular linkage of the Anderson anions. Moreover, high-angle annular dark field scanning TEM (HAADF-STEM) imaging and the corresponding EDS elemental mapping (Figure S3a, Supporting Information) verify the uniform distribution of C, N, O, Cl, Mn, Zn, and Mo throughout 1. Additionally, local selected area electron diffraction (SAED) analysis (Figure S3b, Supporting Information) indicates its crystalline characteristic, and the d-spacing calculated from SAED is 4.83 nm^{-1}, which is indeed in line with the d-spacing value calculated from powder X-ray diffraction (pXRD), which is 4.40 nm^{-1} (Figure S3c, Supporting Information).

In addition, to examine the elemental distribution of Mn, Zn, Cl, and Mo of the bulk material, a small piece of 1, 2D micro X-ray fluorescence spectroscopy (2D-μXRF; resolution ≈25 μm) was employed. Homogeneous distribution of the four elements is reflected by similar intensities, i.e., coloring of the bulk material, notably within the selected area of (1 × 1) mm^2 in the bulk material as indicated by the green square (Figure S5a, Supporting Information). This becomes more obvious when assessing the intensity histograms that were generated for this area (Figure S5b, Supporting Information), displaying a normal distribution of intensities and no extreme values. The parameters of the intensity histograms are listed in (Table S7, Supporting Information), showing relative standard deviations of 9% to max. 20%. In order to investigate possible inhomogeneities in the element composition within the sample, the elemental intensity ratios were calculated along three exemplary lines, each 2.5 to 3.5 mm long. As illustrated in (Figure S6, Supporting Information), a constant elemental ratio with a spread width of less than 0.01 (see insert) was achieved in comparison to a spread width in the range of 2 for the background. Hence, high homogeneity in the elemental distribution and composition within the investigated sample is proven. In addition, EDX analyses showed the expected atomic metal ratios for Mn: Mo (calcd: 1: 6, obsd: 1: 5.6), confirming the presence of the two Anderson-metal components at the expected ratio.

In order to probe the porosity of 1, N_2 sorption studies were performed using Brunauer–Emmett–Teller (BET) and Barrett-Joyner–Halenda (BJH) analysis (**Figure 5**). 1 showed an IUPAC Type III isotherm (Figure 5a),[61] indicating weak interactions between the N_2 gas and the surface of 1. The BET surface area of 15.9 $m^2\ g^{-1}$ and narrow pore size distribution with an average pore diameter of 11.5 nm (Figure 5b) is displayed by 1.

2.2. Oxidation of Benzyl Alcohol, Furfuryl Alcohol and Octanol

POMs have been widely investigated as catalysts for a range of organic oxidation reactions.[62–65] Anderson-type POMs in particular have proven to be efficient catalysts for alcohol oxidation reactions.[66–68] Therefore, we explored the selective heterogeneous oxidation of primary alcohols using benzyl alcohol, furfuryl alcohol, and octanol as substrates with *tert*-butyl hydroperoxide (*t*BuOOH) in decane as an oxidant to study the catalytic performance of 1. In brief, a typical experiment was performed using a stock solution of toluene-d_8 (9.8 mL) containing the corresponding alcohol (1 mmol), and *t*BuOOH (1 mmol), as well as 1 as a heterogeneous catalyst (10 mg). 1 mL of this reaction solution was added to catalytic vials, which were heated at 65 °C for a specific time. After the reaction, the catalyst was separated via centrifugation, and analysis of the products was performed by quantitative ^{1}H NMR spectroscopy (for experimental and characterization details, see Section S2.2 and Figure S7, Supporting Information). For benzyl alcohol oxidation, our data show that in the presence of 1, we observe significantly higher yields of benzaldehyde compared with the blank reference reaction (**Figure 6**a). Similarly, significantly higher furfural and octanal yields were observed in the presence of 1 catalyst (Figure 6b; Figure S8, Supporting Information) over time. These findings suggest that 1 shows higher performance for benzyl alcohol oxidation compared with furfuryl alcohol and octanol

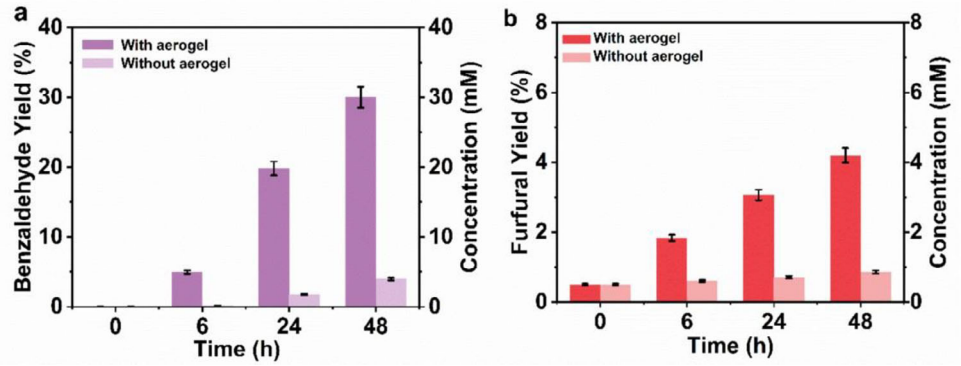

Figure 6. Catalytic oxidation of a) benzyl alcohol; b) furfuryl alcohol. Reaction conditions: catalyst: 1 (10 mg), solvent: toluene-d_8 (9.8 mL), substrate: benzyl alcohol, furfuryl alcohol (1 mmol), oxidant: *t*BuOOH (1 mmol). $T = 65$ °C.

oxidation. This might be related to the more complex structure of furfuryl alcohol and octanol, and mechanistic studies are ongoing.

To further examine the activity of different catalysts under identical conditions, we opted to use benzyl alcohol as a test reaction. Significantly, lower yields of benzaldehyde were observed with various catalysts, whereas catalyst 1 showed a 30% yield of benzaldehyde after 48 h, highlighting that under the given reaction conditions, catalyst 1 is the superior catalyst (Table S8, Supporting Information, entries 1–4). Also, a controlled experiment without *t*BuOOH shows noticeably low benzaldehyde yield, signifying the role of the oxidant in the catalysis (Table S8, Supporting Information, entry 5).

The recyclability of 1 was investigated in four catalytic runs using the benzyl alcohol oxidation as a test reaction. After each run, the catalyst was separated from the reaction solution via centrifugation, washed twice with toluene and diethyl ether, and vacuum dried. Then, the dried catalyst was employed for the subsequent reaction batch. It was noticed that the catalyst can be recovered and reused at least 4 times without a major loss in its catalytic activity (Figure S9, Supporting Information). The observed reduction in benzaldehyde yield might be due to the loss of catalyst during the washing process, as well as the leaching of the catalyst.

2.3. Post-Catalytic Studies

Stability is one of the crucial parameters to evaluate the catalytic performance of a catalyst. Therefore, to gain insights into the stability of 1, we recovered the catalyst after 48 h of the reaction cycle of benzyl alcohol oxidation. The morphology and structural changes of 1 after catalysis were studied by SEM, FT-IR, and XPS. The SEM image of 1 (Figure S10c, Supporting Information) after catalysis displayed that the original layered structure was mostly maintained. Furthermore, the FT-IR spectrum of 1 (Figure S10a, Supporting Information) showed that the positions of characteristic bands of $MnMo_6$ are retained. Deconvoluted XPS data (Figure S11, Supporting Information) revealed the retention of the elemental composition and oxidation states in 1. Moreover, the elemental composition (in at.%) of 1 was calculated from XPS, indicating the leaching of the catalyst (Table S9, Supporting Information). The results suggest that the structural and morphological features of 1 are maintained during catalytic runs.

2.4. Mechanistic Insights of the Gelation

It was observed that the addition of $ZnCl_2$ solution (in MeCN) to the $MnMo_6$ solution (in MeCN) led to the immediate formation of a gel. A systematic investigation was conducted to understand the factors influencing the gel formation, such as POM type, metal salts used, solvent, etc. (for details see Section S2.3, Tables S1–S5, Supporting Information). Attempts to replace $ZnCl_2$ with other metal cations, including transition metals, alkali, and alkaline earth metals, did not result in the formation of a stable gel. However, when $CoCl_2.6H_2O$ was used, we observed the formation of a gel that was unstable and showed syneresis (release of solvent from the gel) over the course of a day. A similar behavior was observed when using $Zn(NO_3)_2.6H_2O$, however, syneresis occurred within a 15 min timeframe. Based on these analyses, we can state that formation of a stable gel under the given conditions is specific to $ZnCl_2$, and both Zn(II) as well as Cl^- are required to form the stable gel. Efforts to substitute acetonitrile with other protic and aprotic organic solvents showed that formation of gel particles was observed when benzonitrile was employed, suggesting that nitrile groups might be involved in the gelation process. Also, a variety of POM anions were tested; however, only the TRIS-bearing Anderson POM resulted in gelation.

3. Conclusion

In summary, we have demonstrated a facile approach to synthesize 1 based on TRIS-functionalized Anderson polyoxometalate anions as low molecular weight gelators when crosslinked with $ZnCl_2$ in acetonitrile. The resulting gel showed promising initial alcohol oxidation reactivity for benzyl alcohol and the bio-based furfuryl alcohol. Initial insights into the individual roles of POM anion, metal salt, and solvent are provided to guide the future development of this new class of POM-based porous catalyst.

Supporting Information

Supporting Information is available from the Wiley Online Library or from the author.

Acknowledgements

This work was funded by the Deutsche Forschungsgemeinschaft via the Transregio SFB TRR 234 "CataLight", projects no A4, B3, B7, B8, Z2 (project no: 364549901) and the SFB 1633 "PCET" (project no: 510228793). S. A. C. and D.A. gratefully acknowledge financial support from the Alexander von Humboldt Foundation. C.S. gratefully acknowledges financial support from the Top-Level Research Area SunInnoScience and the Gutenberg Research College. The authors gratefully acknowledge Daniel Hönders and Prof. Andreas Walther, JGU Mainz, for instrumental access.

Open access funding enabled and organized by Projekt DEAL.

Conflict of Interest

The authors declare no conflict of interest.

Data Availability Statement

The data that support the findings of this study are openly available in zenodo.org at https://doi.org/10.5281/zenodo.15771544, reference number 15771544.

Keywords

aerogel, organofunctionalization, polyoxometalate, porosity, self-assembly

Received: June 30, 2025
Revised: August 28, 2025
Published online: September 24, 2025

[1] T. Christoff-Tempesta, A. J. Lew, J. H. Ortony, *Gels* **2018**, *4*, 40.
[2] D. K. Smith, *Soft Matter* **2023**, *20*, 10.
[3] N. M. Sangeetha, U. Maitra, *Chem. Soc. Rev.* **2005**, *34*, 821.
[4] G. Picci, C. Caltagirone, A. Garau, V. Lippolis, J. Milia, J. W. Steed, *Coord. Chem. Rev.* **2023**, *492*, 215225.
[5] A. Fortunato, M. Mba, *Gels* **2021**, *7*, 85.
[6] M. M. Piepenbrock, G. O. Lloyd, N. Clarke, J. W. Steed, *Chem. Rev.* **2010**, *110*, 1960.
[7] J. W. Steed, *Chem. Soc. Rev.* **2010**, *39*, 3686.
[8] J. Zhang, C. Y. Su, *Coord. Chem. Rev.* **2013**, *257*, 1373.
[9] S. Dhibar, A. Dey, D. Ghosh, S. Majumdar, A. Dey, P. P. Ray, B. Dey, *ACS Omega* **2020**, *5*, 2680.
[10] Q. Lin, T. T. Lu, X. Zhu, B. Sun, Q. P. Yang, T. B. Wei, Y. M. Zhang, *Chem. Commun.* **2015**, *51*, 1635.
[11] P. Grondin, O. Roubeau, M. Castro, H. Saadaoui, A. Colin, R. Clérac, *Langmuir* **2010**, *26*, 5184.
[12] A. Roy, S. Dhibar, S. Kumar, S. Some, P. Garg, P. Ruidas, S. Bhattacharjee, A. Bera, B. Saha, S. J. Ray, *Sci. Rep.* **2024**, *14*, 31619.
[13] S. Dhibar, A. Dey, A. Dalal, S. Bhattacharjee, R. Sahu, R. Sahoo, A. Mondal, S. Mehebub Rahaman, S. Kundu, B. Saha, *J. Mol. Liq.* **2023**, *370*, 121021.
[14] A. Gasnier, G. Royal, P. Terech, *Langmuir* **2009**, *25*, 8751.
[15] P. Terech, M. Yan, M. Maréchal, G. Royal, J. Galvez, S. K. P. Velu, *Phys. Chem. Chem. Phys.* **2013**, *15*, 7338.
[16] S. S. Sonu, N. Rai, I. Chauhan, *J. Sol-Gel Sci. Technol.* **2023**, *105*, 324.
[17] X. Jiang, R. Du, R. Hübner, Y. Hu, A. Eychmüller, *Matter* **2021**, *4*, 54.
[18] R. C. Walker, A. E. Potochniak, A. P. Hyer, J. K. Ferri, *Adv. Colloid Interface Sci.* **2021**, *295*, 102464.
[19] I. Smirnova, P. Gurikov, *J. Supercrit. Fluids* **2018**, *134*, 228.
[20] G. Wang, X. Li, X. Yang, L. X. Liu, Y. Cai, Y. Wu, S. Wang, H. Li, Y. Zhou, Y. Wang, Y. Zhou, *Chem. - Eur. J.* **2022**, *28*, 202201834.
[21] L. E. Nita, A. Ghilan, A. G. Rusu, I. Neamtu, A. P. Chiriac, L. E. Nita, A. Ghilan, A. G. Rusu, I. Neamtu, A. P. Chiriac, *Pharmaceutics* **2020**, *12*, 449.
[22] J. Mao, J. Iocozzia, J. Huang, K. Meng, Y. Lai, Z. Lin, *Energy Environ. Sci.* **2018**, *11*, 772.
[23] R. Ganesamoorthy, V. K. Vadivel, R. Kumar, O. S. Kushwaha, H. Mamane, *J. Clean Prod.* **2021**, *329*, 129713.
[24] N. R. Khan, T. Sharmin, A. B. Rashid, *Heliyon* **2024**, *10*, 23102.
[25] W. Liu, A. K. Herrmann, N. C. Bigall, P. Rodriguez, D. Wen, M. Oezaslan, T. J. Schmidt, N. Gaponik, A. Eychmüller, *Acc. Chem. Res.* **2015**, *48*, 154.
[26] Y. Hu, H. Zhuo, Z. Chen, X. Peng, L. Zhong, R. Sun, *J. Mater. Sci. Technol.* **2021**, *71*, 67.
[27] H. Zhang, W. Han, K. Xu, Y. Zhang, Y. Lu, Z. Nie, Y. Du, J. Zhu, W. Huang, *Nano Lett.* **2020**, *20*, 3449.
[28] Q. Liu, X. Wang, *Matter* **2020**, *2*, 816.
[29] S. Guo, C. W. Pan, M. Hou, Y. T. Hou, S. Yao, T. B. Lu, Z. M. Zhang, *Angew. Chem., Int. Ed.* **2025**, *64*, 202420398.
[30] Z. R. Zhang, H. Y. Sui, W. X. Shi, J. Ren, S. Yao, Lu, T. B. L.u, Z. M. Zhang, *Angew. Chem., Int. Ed.* **2025**, *64*, 202416711.
[31] B. Li, L. Xuan, L. Wu, *Macromol. Rapid Commun.* **2022**, *43*, 2200019.
[32] X. Meng, H. N. Wang, Y. H. Zou, L. S. Wang, Z. Y. Zhou, *Dalton Trans.* **2019**, *48*, 10422.
[33] M. S. Centellas, M. Piot, R. Salles, A. Proust, L. Tortech, D. Brouri, S. Hupin, B. Abécassis, D. Landy, C. Bo, G. Izzet, *Chem. Sci.* **2020**, *11*, 11072.
[34] A. Blazevic, A. Rompel, *Coord. Chem. Rev.* **2016**, *307*, 42.
[35] S. Favette, B. Hasenknopf, J. Vaissermann, P. Gouzerh, C. Roux, *Chem. Commun.* **2003**, *59*, 2664.
[36] Z. He, H. Wang, Y. Wang, Y. Wu, H. Li, L. Bi, L. Wu, *Soft Matter* **2012**, *8*, 3315.
[37] L. Casimiro, F. Volatron, G. Boivin, B. Abécassis, S. Alves, D. Brouri, D. Montero, J. M. Guigner, L. M. Chamoreau, G. Gontard, D. Portehault, Y. Li, A. Proust, R. Lescouëzec, G. Ducouret, A. Solé-Daura, P. Davidson, T. Merland, G. Izzet, *JACS Au* **2024**, *4*, 4948.
[38] C. Dong, X. Liu, Z. Li, K. Guo, C. Song, Y. Zhang, M. Zhang, F. Ma, F. Rosei, X. Zhang, X. Huang, *Adv. Funct. Mater.* **2024**, *35*, 2418410.
[39] L. Ni, G. Yang, C. Sun, G. Niu, Z. Wu, C. Chen, X. Gong, C. Zhou, G. Zhao, J. Gu, W. Ji, X. Huo, M. Chen, G. Diao, *Mater. Today Energy* **2017**, *6*, 53.
[40] F. Yahya, H. El-Rassy, G. Younes, R. Al-Oweini, *Desal. Water Treat.* **2020**, *195*, 321.
[41] T. Liu, Y. Zhang, C. Wang, Y. Kang, M. Wang, F. Wu, W. Huang, *Small* **2024**, *20*, 2308378.
[42] R. Song, X. Zhang, H. Wang, C. Liu, *Molecules* **2022**, *27*, 2782.
[43] S. Wang, X. Wang, X. Y. Shi, C. X. Meng, C. L. Sun, Z. S. Wu, *New Carbon Mater.* **2021**, *36*, 189.
[44] Y. Wang, X. Kong, W. Xu, F. Jiang, B. Li, L. Wu, *Inorg. Chem.* **2018**, *57*, 3731.
[45] J. C. Raabe, T. Esser, M. J. Poller, J. Albert, *Catal. Today* **2024**, *441*, 114899.
[46] P. R. Marcoux, B. Hasenknopf, J. Vaissermann, P. Gouzerh, *Eur. J. Inorg. Chem.* **2003**, *2003*, 2406.
[47] S. R. Raghavan, B. H. Cipriano, *Gel Formation: Phase Diagrams Using Tabletop Rheology and Calorimetry*, (Eds.: R.G. Weiss, P. Terech), Springer, Dordrecht **2005**, pp. 241–252.
[48] S. C. Karunakaran, B. J. Cafferty, K. S. Jain, G. B. Schuster, N. V. Hud, *ACS Omega* **2020**, *5*, 344.
[49] P. Venkateswaslu, *J. Chem. Phys.* **1952**, *20*, 923.
[50] E. L. Pace, L. J. Noe, *J. Chem. Phys.* **1968**, *49*, 5317.

[51] S. Khlifi, S. Yao, C. Falaise, P. Bauduin, V. Guérineau, N. Leclerc, M. Haouas, H. Salmi-Mani, P. Roger, E. Cadot, *Chem. - Eur. J.* **2024**, *30*, 202303815.
[52] S. Mahvash, V. A. Zavareh, S. Taymouri, M. Mirian, M. Ramezani-Aliakbari, F. Dousti, M. Rostami, *J. Drug Deliv. Sci. Technol.* **2023**, *87*, 104778.
[53] F. Jones, H. Tran, D. Lindberg, L. Zhao, M. Hupa, *Energy and Fuels* **2013**, *27*, 5663.
[54] N. Tancredi, M. Gabús, M. I. Yoshida, A. C. Suárez, *Eur. J. Wood Wood Prod.* **2017**, *75*, 633.
[55] A. Marciel, M. Graça, A. Bastos, L. Pereira, J. S. Kumar, J. Borges, F. Vaz, M. Peres, S. Magalhães, K. Lorenz, R. Silva, *Materials* **2021**, *14*, 821.
[56] C. Peng, T. Chen, B. Zeng, G. Chen, C. Yuan, Y. Xu, L. Dai, *Compos. B Eng.* **2020**, *186*, 107780.
[57] Z. Y. Tian, P. Mountapmbeme Kouotou, N. Bahlawane, P. H. Tchoua Ngamou, *J. Phys. Chem. C* **2013**, *117*, 6218.
[58] D. Hoang, Y. Li, M. S. Jung, S. K. Sandstrom, A. M. Scida, H. Jiang, T. C. Gallagher, B. A. Pollard, R. Jensen, N. C. Chiu, K. Stylianou, W. F. Stickle, P. A. Greaney, X. Ji, *Adv. Energy Mater.* **2023**, *13*, 1.
[59] S. A. Schmidt, N. Kumar, A. Shchukarev, K. Eränen, J. P. Mikkola, D. Y. Murzin, T. Salmi, *Appl. Catal. A Gen.* **2013**, *468*, 120.
[60] L. Han, S. Song, M. Liu, S. Yao, Z. Liang, H. Cheng, Z. Ren, W. Liu, R. Lin, G. Qi, X. Liu, Q. Wu, J. Luo, H. L. Xin, X. Liu, Q. Wu, J. Luo, H. L. Xin, *J. Am. Chem. Soc.* **2020**, *142*, 12563.
[61] M. Thommes, K. Kaneko, A. V. Neimark, J. P. Olivier, F. Rodriguez-Reinoso, J. Rouquerol, K. S. W. Sing, *Pure Appl. Chem.* **2015**, *87*, 1051.
[62] C. L. Hill, C. M. Prosser-McCartha, *Coord. Chem. Rev.* **1995**, *143*, 407.
[63] Z. Wei, J. Wang, H. Yu, S. Han, Y. Wei, *Molecules* **2022**, *27*, 5212.
[64] D. Barats, R. Neumann, *Adv. Synth. Catal.* **2010**, *352*, 293.
[65] A. M. Khenkin, L. J. W. Shimon, R. Neumann, *Inorg. Chem.* **2003**, *42*, 3331.
[66] Y. Wang, Z. Wu, H. Yu, S. Han, Y. Wei, *Green Chem.* **2020**, *22*, 3150.
[67] M. Zhang, Y. Zhai, S. Ru, D. Zang, S. Han, H. Yu, Y. Wei, *Chem. Commun.* **2018**, *54*, 10164.
[68] Z. Wei, S. Ru, Q. Zhao, H. Yu, G. Zhang, Y. Wei, *Green Chem.* **2019**, *21*, 4069.